European Radiology (2019) 29:6643–6652
https://doi.org/10.1007/s00330-019-06203-x

MAGNETIC RESONANCE

Amide proton transfer imaging might predict survival and IDH mutation status in high-grade glioma

Bio Joo[1] · Kyunghwa Han[1] · Sung Soo Ahn[1] · Yoon Seong Choi[1] · Jong Hee Chang[2] · Seok-Gu Kang[2] · Se Hoon Kim[3] · Jinyuan Zhou[4] · Seung-Koo Lee[1]

Received: 8 November 2018 / Revised: 14 March 2019 / Accepted: 26 March 2019 / Published online: 3 June 2018

Abstract

Objectives To assess the utility of amide proton transfer (APT) imaging as an imaging biomarker to predict prognosis and molecular marker status in high-grade glioma (HGG, WHO grade III/IV).

Methods We included 71 patients with pathologically diagnosed HGG who underwent preoperative MRI with APT imaging. Overall survival (OS) and progression-free survival (PFS) according to APT signal, clinical factors, MGMT methylation status, and IDH mutation status were analyzed. Multivariate Cox regression models with and without APT signal data were constructed. Model performance was compared using the integrated AUC (iAUC). Associations between APT signals and molecular markers were assessed using the Mann-Whitney test.

Results High APT signal was a significant predictor for poor OS (HR = 3.21, 95% CI = 1.62–6.34) and PFS (HR = 2.22, 95% CI = 1.33–3.72) on univariate analysis. On multivariate analysis, high APT signals were an independent predictor of poor OS and PFS when clinical factors alone (OS: HR = 2.89; PFS: HR = 2.13), or in combination with molecular markers (OS: HR = 2.85; PFS: HR = 2.00), were included as covariates. The incremental prognostic value of APT signals was significant for OS and PFS. IDH-wild type was significantly associated with high APT signals ($p = 0.001$) when compared to IDH-mutant; however, there was no difference based on MGMT methylation status ($p = 0.208$).

Conclusion High APT signal was a significant predictor of poor prognosis in HGG. APT data showed significant incremental prognostic value over clinical prognostic factors and molecular markers and may also predict IDH mutation status.

Key Points

- *Amide proton transfer (APT) imaging is a promising prognostic marker of high-grade glioma.*
- *APT signals were significantly higher in IDH-wild type compared to IDH-mutant high-grade glioma.*
- *APT imaging may be valuable for preoperative screening and treatment guidance.*

Keywords Glioma · Magnetic resonance imaging · Isocitrate dehydrogenase · Prognosis

Abbreviations

APT	Amide proton transfer
AUC	Area under the curve
CCRT	Concurrent chemoradiation therapy
HGG	High-grade glioma
iAUC	Integrated area under the curve
ICC	Intraclass correlation coefficients
IDH	Isocitrate dehydrogenase
KPS	Karnofsky performance status
MGMT	O^6-methylguanine-DNA methyltransferase
MRI	Magnetic resonance imaging
MTR_{asym}	Magnetization transfer ratio asymmetry

✉ Sung Soo Ahn
SUNGSOO@yuhs.ac

[1] Department of Radiology and Research Institute of Radiological Science, Yonsei University College of Medicine, 50 Yonsei-ro, Seodaemun-gu, Seoul 120-752, South Korea

[2] Department of Neurosurgery, Yonsei University College of Medicine, Seoul, South Korea

[3] Department of Pathology, Yonsei University College of Medicine, Seoul, South Korea

[4] Division of MRI Research, Department of Radiology, Johns Hopkins University School of Medicine, Baltimore, MD, USA

OS Overall survival
PCR Polymerase chain reaction
PFS Progression free survival
ROI Region of interests

Introduction

Glioma is a common primary brain tumor in adults [1]. High-grade gliomas (HGG, WHO grade III/IV gliomas) are malignant tumors that have poor prognosis despite aggressive treatment, including surgery and adjuvant concurrent chemoradiation therapy with temozolomide. The median survival is approximately 3.5 years for anaplastic astrocytoma and 15 months for glioblastoma [2].

Clinical factors, such as age, Karnofsky performance status (KPS) score, extent of tumor resection, and treatment modality, are standard prognostic factors for glioma; younger age, higher KPS, gross total resection of tumor, and adjuvant concurrent chemoradiation therapy with temozolomide showed better survival [3–5]. Recently, molecular markers, including isocitrate dehydrogenase (IDH) mutation, O^6-methylguanine-DNA methyltransferase (MGMT) promotor methylation, 1p19q codeletion, TP53, TERT, EGFR amplification, and ATRX have been correlated with glioma prognosis [6–11]. Especially, IDH mutation and MGMT promoter methylation have been discovered as critical prognostic molecular markers for gliomas [12, 13]. IDH mutation occurs in the majority of WHO grade II/III gliomas and secondary glioblastomas and carries a favorable clinical prognosis [14, 15]. Hence, IDH mutation status was integrated to the recent 2016 WHO classification of central nervous system tumors [16]. IDH gene–encoded enzymes catalyze oxidative decarboxylation of isocitrate into α-ketoglutarate, generating NADPH which is important for the defense mechanism against oxidative damage, whereas IDH mutation causes the conversion of α-ketoglutarate into D-2-hydroxyglutarate while consuming NADPH [17]. Thus, IDH mutation in tumor cells is thought to lead to an increased susceptibility to oxidative damage which occurs during treatment using irradiation and/or chemotherapy, resulting in prolonged survival [18]. On the other hand, MGMT promoter methylation blocks MGMT protein expression and is associated with better responses to temozolomide therapy and, consequently, is associated with a better prognosis than the unmethylated promoter status [19].

Several studies have investigated the efficacy of conventional and advanced MRI for preoperative prognostication of gliomas, reporting the association of prognosis and perfusion MRI parameters or apparent diffusion coefficient. Although those results are promising, there are still controversies regarding the prognostic values of preoperative imaging because of varying results depending on the disease entity and grade, metrics, and analysis method [20–23].

Amide proton transfer (APT) imaging is a specific type of chemical exchange saturation transfer (CEST) imaging which indirectly detects molecules in the millimolar range without exogenous contrast agents by using the chemical exchange between protons of proteins/peptides and water pool protons [24, 25]. In APT imaging, selective saturation of amide protons of solute molecules is achieved by 3.5-ppm downfield off-resonance radiofrequency (RF) irradiation and transferred to water pool protons by chemical exchange, resulting in reduction of water signal intensity and, eventually, generating image contrast [26]. Several reports suggest that APT signals are a promising imaging biomarker for glioma grading and prediction of molecular marker status [27–31]. Additionally, a recent study investigated the utility of APT imaging for predicting treatment response in glioblastoma patients [32]. Thus far, however, no study has reported on the applicability of APT imaging for prognostication of HGG.

Therefore, this study aimed to assess the utility of APT imaging as a prognostic biomarker in HGG. We also investigated the ability of APT signals to predict IDH mutation and MGMT promoter methylation status in HGG.

Materials and methods

Our institutional review board approved this retrospective study and waived the requirement for informed consent.

Study population

We reviewed the records of 72 consecutive patients who underwent preoperative MRI with APT imaging for newly diagnosed HGG from November 2014 to May 2018. The inclusion criteria were ≥ 20 years old, pathologically confirmed HGG, and no prior biopsy or treatment. The exclusion criteria were previous brain biopsy or treatments, unavailable IDH mutation or MGMT methylation status, and inadequate APT imaging quality. One patient was excluded because of inadequate APT imaging quality leading to processing errors. Thus, 71 patients were enrolled. The interval between MRI and surgery was less than 1 week for all patients.

Image acquisition

MRI was performed using a 3-Tesla system (Achieva until 2016 and Ingenia thereafter, Philips Medical Systems) and a 32-channel receiver head coil with a body transmit coil. APT imaging was acquired using the three-dimensional gradient- and spin-echo approach with the following parameters: voxel size, 2.2 × 2.2 mm; slice thickness, 4.4 mm; repetition time (TR), 3000 ms; echo time (TE), 17 ms; turbo spin-echo factor, 22; echo planar imaging factor, 7; and number of slices, 15. Using four repetitions at six saturation-frequency offsets

(± 3.0, ± 3.5, and ± 4.0 ppm), a sufficient signal-to-noise ratio could be achieved within a clinical time frame. APT imaging was conducted with an RF saturation amplitude of 2 μT and total duration of 800 ms, which consisted of a four-block pulsed saturation scheme. The water frequency shift due to field inhomogeneity was measured in a separate scan using the water saturation shift referencing method with 21 offset frequencies ranging from − 1.25 to 1.25 ppm, at a step of 0.125 ppm (16 Hz), and one reference scan without a saturation RF pulse resulting in a full z spectrum within the offset range [33]. This scan was acquired with a TR/TE of 1250 ms/17 ms, RF saturation amplitude of 0.5 μT, total duration of 400 ms consisting of a two-block pulsed saturation scheme, and the same imaging parameters as those used in APT imaging. The total acquisition time for both the APT and water saturation shift referencing scans was 7 min and 40 s. Except for the change of scanners, the image acquisition method was kept constant without modification over the whole period.

The conventional MRI sequences included axial T1-weighted (TR/TE, 2000 ms/10 ms; FOV, 240 mm; slice thickness, 5 mm; matrix, 256 × 256); axial T2-weighted (TR/TE, 3000 ms/80 ms; FOV, 240 mm; slice thickness, 5 mm; matrix, 256 × 256); and axial fluid-attenuated inversion recovery imaging (TR/TE, 10,000 ms/125 ms; FOV, 240 mm; slice thickness, 5 mm; matrix, 256 × 256). Three-dimensional post-contrast T1-weighted images (TR/TE, 6.3 ms/3.1 ms; FOV, 240 mm; slice thickness, 1 mm; matrix, 192 × 192) were also acquired.

Image processing and analysis

After water frequency shift correction, we calculated magnetization transfer ratio asymmetry (MTR_{asym}) values at ± 3.5 ppm with respect to water frequency:

$$MTR_{asym}(+3.5ppm) = \frac{S_{sat}(-3.5ppm) - S_{sat}(+3.5ppm)}{S_0},$$

where S_0 and S_{sat} (± 3.5 ppm) are MRI signals without and with saturation RF pulse, respectively.

The full water saturation shift referencing z spectrum was fitted to a 12th-order polynomial at each voxel, and the lowest signal in the fit after interpolation at a higher spectral resolution (1 Hz) was assumed to be the actual water resonance frequency, resulting in a water center frequency offset at a corresponding voxel. The acquired APT data were organized according to the offsets, and saturation images with the same offsets were averaged. The offset data for each voxel were interpolated over a frequency offset range and shifted using the fitted water saturation shift referencing central frequency offset at the same voxel. Based on the shift-corrected data, the APT-weighted signal parameter map was generated using an MTR_{asym} at ± 3.5 ppm. Post-processing of APT images was performed with Matlab (MathWorks).

One circular ROI was drawn on the APT-weighted images for each patient by two neuroradiologists (YSC and SSA, with 5 and 10 years of experience in neuroradiology, respectively) who were blinded to clinical and histopathological data. Each ROI was manually placed in a place in the solid portion of tumor that best represented the entire tumor signal on raw APT images. Careful attempts were made to include the areas showing the highest signal on APT-weighted images and to exclude cystic or necrotic portions by referring to both T2-weighted and post-contrast T1-weighted images. Each ROI was then transferred to proceeded APT-weighted images using the Medical Image Processing, Analysis, and Visualization software package (MIPAV, version 7.0; National Institutes of Health). The reason why we put ROI on the raw APT images instead of the proceeded APT-weighted images was that it was difficult to distinguish a solid portion from a cystic or necrotic portion on the APT-weighted images. The mean ROI values from the APT-weighted images were analyzed. The ROI size at each lesion ranged from 242 to 290.4 mm^2.

Surgery and pathological evaluation

All patients underwent surgical tumor resection or biopsy after MRI. Pathological diagnosis was made by neuropathologists according to the 2016 WHO classification of central nervous system tumors [16]. Immunohistochemical analysis and peptide nucleic acid–mediated clamping polymerase chain reaction (PCR) were performed to detect the IDH1 R132H mutation. We used the monoclonal antibody H09 for immunohistochemical analysis, and IDH1-R132H positive staining was determined as positive in patients with any stained cells [34]. When patients were negative for IDH1-R132H immunopositivity, we confirmed IDH1/2 status including rarer mutations other than IDH1-R132H by peptide nucleic acid–mediated clamping PCR. MGMT promoter methylation status was assessed on the basis of methylation-specific PCR.

Additional prognostic parameters

Age, sex, preoperative KPS, postoperative treatment, and extent of tumor resection were recorded. The extent of tumor resection was classified as total, subtotal (< 100% and ≥ 75% of gross total removal), or partial (< 75% of gross tumor removal) resection or biopsy based on the surgeon's intraoperative impressions in conjunction with postoperative MRI findings. Postoperative treatment was categorized as concurrent chemoradiation with temozolomide (CCRT), radiation therapy only, temozolomide-based chemotherapy only, and no postoperative treatment.

Survival time

Overall survival (OS) was defined as the time from diagnosis to death or the date of the last follow-up examination if the patient did not die. Progression-free survival (PFS) was defined as the time from diagnosis to tumor progression, death, or the date of the last follow-up examination if the patient did not show disease progression or die. Tumor progression was defined based on the following response assessment: (a) an increase of ≥ 25% in size of enhancing tumor within the radiation field was seen on at least two consecutive follow-up MRI examinations or pathologically proved to be tumor recurrence; (b) a newly appearing enhancing lesion was seen outside the radiation field; (c) clinical deterioration secondary to disease was observed; or (d) death in patients who did not meet the above criteria. Image analysis to determine the date of tumor progression was performed based on the consensus of two neuroradiologists (YSC and SSA, with 5 and 10 years of experience in brain MRI, respectively).

Statistical analysis

Inter-observer reliability of APT signal measurements between the two radiologists was evaluated by intraclass correlation coefficients (ICC); ICC > 0.75 indicated excellent agreement.

Univariate survival analyses of APT signals for OS and PFS were performed with Kaplan-Meier estimates and the log-rank test. For the analysis, the APT signal was dichotomized using optimal cutoff values that were calculated from the "cutp" function of the "survMisc" R package (R Foundation for Statistical Computing) on the basis of the score test from the Cox regression model. Univariate analyses were then performed on all factors (age, KPS, extent of tumor resection, MGMT methylation status, IDH mutation status, postoperative treatment, and APT signal) for OS and PFS using Cox regression analysis. The extent of tumor resection (total resection vs. otherwise) was dichotomized without further grouping because most of the patients (87.3%) underwent the total resection. Postoperative treatment (CCRT vs. otherwise) was also dichotomized.

Multivariate Cox regression analysis was used to build prognostic models for OS and PFS. First, we investigated the additional prognostic value of the APT signal when it is combined with important clinical factors, such as age, KPS, and extent of tumor resection. The prognostic models for OS and PFS were established using the important clinical factors only (model 1); then, the APT signal was added as a covariate (model 2). Next, molecular markers that were significant ($p < 0.05$) in the univariate analysis as well as important clinical factors were included as covariates to build prognostic models (model 3). Finally, the APT signal was added to model 3 to assess the additional prognostic value (model 4).

We compared the predictive performance of each pair of models with and without APT signal data (model 1 vs. 2 and model 3 vs. 4) for OS and PFS by calculating the integrated AUC (iAUC), using the "risksetROC" R package [35]. Bootstrapping with 1000 repetition sampling was used to calculate the 95% confidence interval of the difference of iAUC

Table 1 Clinical characteristics of the patients

Age (year)	50.6 ± 15.7	
Sex		
Male	37	(52.1%)
Female	34	(47.9%)
KPS	79.6 ± 11.0	
Extent of resection		
Total	62	(87.3%)
Subtotal	4	(5.6%)
Partial	1	(1.4%)
Biopsy	4	(5.6%)
Postoperative treatment		
CCRT	47	(66.2%)
Radiation therapy only	20	(28.2%)
Chemotherapy only	2	(2.8%)
No postoperative treatment	2	(2.8%)
Histopathology		
Grade III	20	(28.2%)
Anaplastic astrocytoma, IDH-mutant	5	(7.0%)
Anaplastic astrocytoma, IDH-wild type	9	(12.7%)
Anaplastic oligodendroglioma, IDH-mutant and 1p/19q codeleted	6	(8.5%)
Grade IV	51	(71.8%)
Glioblastoma, IDH-wild type	49	(69.0%)
Glioblastoma, IDH-mutant	1	(1.4%)
Diffuse midline glioma	1	(1.4%)
IDH mutation		
IDH-mutant	13	(18.3%)
IDH-wild type	58	(81.7%)
MGMT methylation		
Methylated	25	(35.2%)
Unmethylated	46	(64.8%)
APT signal (%)		
Mean	2.23 ± 0.776	
Median*	2.30	(1.83–2.76)
OS (days)*	779	(195–759)
Number of deaths	27	(38.0%)
PFS (days)*	483	(171–594)
Number of tumor progression	37	(52.1%)

Age, KPS, and APT signal data are presented as the mean ± standard deviation. *Median (interquartile range). *KPS* = Karnofsky performance status score. *CCRT* = concurrent chemoradiation therapy. *IDH* = isocitrate dehydrogenase. *MGMT* = O^6-methylguanine-DNA methyltransferase. *APT* = amide proton transfer. *OS* = overall survival. *PFS* = progression-free survival

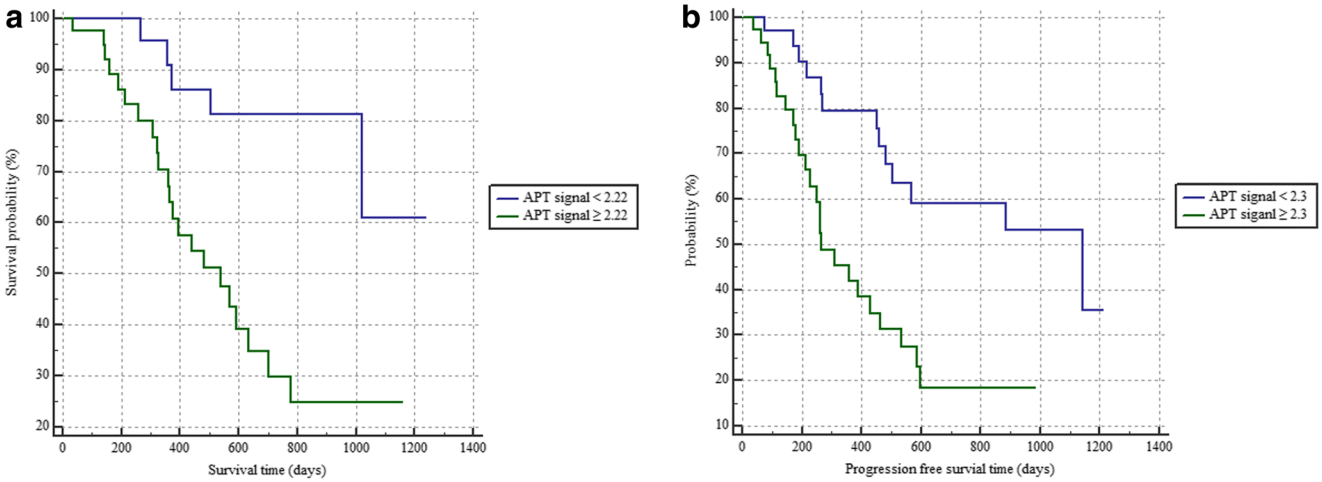

Fig. 1 Kaplan-Meier survival curves for OS (**a**) and PFS (**b**) in patients with HGG. For patients with HGG, the OS and PFS rates were significantly lower for patients with higher APT signal than with lower APT signal ($p < 0.001$ and $p = 0.002$, respectively), when cutoff values of 2.22 and 2.30, respectively, were used as the optimal values

between the two models. The bootstrap procedure, with 1000 bootstrap sampling repetitions, was employed for the iAUC comparisons for internal validation of the prognostic models.

After normality testing, differences in APT signal according to IDH mutation and MGMT methylation status were assessed using the Mann-Whitney test. Statistical analyses were performed using MedCalc (version 9.3.6.0; MedCalc Software) and R (version 3.3.1; R Foundation for Statistical Computing). Statistical significance was set at $p < 0.05$.

Results

The patients' clinical characteristics are summarized in Table 1. Among 71 HGG patients, 20 patients had grade III gliomas and 51 patients had grade IV gliomas. The median follow-up time was 483 days (interquartile range, 195–807 days). The median OS and PFS were 779 days and 483 days, respectively. The number of deaths and tumor progression were 27 (38.03%) and 37 (52.11%), respectively. The mean APT signal was 2.23%. Interrater reliability showed almost perfect reproducibility for APT signal with intraclass correlation coefficients of 0.94 (95% confidence interval [CI] 0.90, 0.96).

The Kaplan-Meier method revealed that a higher APT signal was a significant predictor of poor OS ($p < 0.001$) and PFS ($p = 0.002$), when the cutoff values of 2.22 and 2.30, respectively, were used as the optimal values (Fig. 1). The univariate analysis with Cox regression analysis revealed that older age ($p = 0.009$), unmethylated MGMT ($p = 0.013$), IDH-wild type ($p = 0.024$), and higher APT signal ($p < 0.001$) were significant predictors of poor OS (Table 2). Furthermore, older age ($p = 0.010$), IDH-wild type ($p = 0.011$), and higher APT signal ($p = 0.002$) were significant predictors of poor PFS. Unmethylated MGMT showed a tendency to indicate poor PFS ($p = 0.074$).

Based on the results of univariate analysis, four models for predicting OS and PFS were built, respectively (Tables 3 and 4). The multivariate analysis revealed that APT was the only independent prognostic factor for both OS and PFS among the tested factors. Representative images are depicted in Figs. 2, 3, and 4.

Table 2 Univariate survival analysis

	OS		PFS	
	Hazard ratio (95% CI)	*p* value	Hazard ratio (95% CI)	*p* value
Age	1.032 (1.008, 1.058)	0.009	1.029 (1.007, 1.051)	0.010
KPS	0.983 (0.949, 1.019)	0.346	0.985 (0.957, 1.014)	0.304
Extent of tumor resection	0.446 (0.128, 1.552)	0.205	0.450 (0.170, 1.190)	0.108
MGMT methylation status	0.291 (0.110, 0.771)	0.013	0.513 (0.247, 1.068)	0.074
IDH mutation status	0.100 (0.014, 0.740)	0.024	0.213 (0.065, 0.700)	0.011
Postoperative CCRT	0.910 (0.416, 1.991)	0.813	0.876 (0.450, 1.722)	0.701
APT signal	3.205 (1.621, 6.337)	< 0.001	2.223 (1.330, 3.718)	0.002

KPS = Karnofsky performance status score. *MGMT* = O^6-methylguanine-DNA methyltransferase. *IDH* = isocitrate dehydrogenase. *CCRT* = concurrent chemoradiation therapy. *APT* = amide proton transfer. *OS* = overall survival. *PFS* = progression-free survival

Table 3 Multivariate prognostic models, with and without APT imaging data, for predicting OS

Parameters	Model 1		Model 2		Model 3		Model 4	
	HR	*p* value	HR	*p* value	HR	*p* value	HR	*p* value
Age	1.03 (1.01, 1.06)	0.011	1.02 (0.99, 1.05)	0.149	1.02 (0.99, 1.05)	0.133	1.01 (0.98, 1.04)	0.414
KPS	0.98 (0.95, 1.02)	0.275	0.99 (0.95, 1.02)	0.413	0.99 (0.96, 1.02)	0.440	0.99 (0.96, 1.02)	0.522
Extent of resection	0.51 (0.14, 1.83)	0.303	0.40 (0.11, 1.50)	0.174	0.41 (0.11, 1.47)	0.170	0.33 (0.09, 1.21)	0.094
MGMT methylation					0.41 (0.15, 1.10)	0.075	0.41 (0.15, 1.12)	0.082
IDH mutation					0.17 (0.02, 1.39)	0.099	0.26 (0.03, 2.14)	0.211
APT signal			2.89 (1.34, 6.00)	0.005			2.85 (1.26, 6.41)	0.012
Original iAUC	0.679 (0.567, 0.789)		0.756 (0.664, 0.848)		0.739 (0.659, 0.819)		0.792 (0.714, 0.867)	
Difference of iAUC	0.077 (0.002, 0.194)				0.053 (0.001, 0.134)			
Bootstrapped iAUC	0.708 (0.605, 0.833)		0.788 (0.692, 0.985)		0.801 (0.689, 0.924)		0.860 (0.748, 1.007)	
Difference of bootstrapped iAUC	0.080 (0.023, 0.205)				0.058 (0.011, 0.138)			

Numbers in parentheses indicate the 95% confidence interval. *HR* = hazard ratio. *KPS* = Karnofsky performance status score. *MGMT* = O^6-methylguanine-DNA methyltransferase. *IDH* = isocitrate dehydrogenase. *APT* = amide proton transfer. *iAUC* = integrated AUC

The iAUC comparisons of each pair of models (model 1 vs. 2; model 3 vs. 4) for OS and PFS are presented in Tables 3 and 4. For both OS and PFS, models 2 and 4 showed significantly better performance than models 1 and 3, respectively. The results of internal validation analyses using bootstrapping with 1000 sampling repetitions also showed the same tendency (Tables 3 and 4).

Mann-Whitney tests revealed that IDH-wild type status was significantly associated with high APT signals when compared to IDH-mutant status ($p = 0.001$). Conversely, there was no significant difference in APT signals based on MGMT methylation status ($p = 0.208$) (Table 5).

Discussion

In this study, we found that APT signals had significant prognostic value for predicting OS and PFS in patients with HGG, with high APT signals indicating poor prognosis. When the APT signal was included in the models for predicting OS and PFS, the performance of the models was better than when clinical factors alone or clinical factors and molecular markers were used. Furthermore, we found that the APT signal is significantly associated with IDH mutation status.

It is assumed that the CEST signal indicates the concentration of exchangeable protons in mobile proteins and peptides

Table 4 Multivariate prognostic models, with and without APT imaging data, for predicting PFS

Parameters	Model 1		Model 2		Model 3		Model 4	
	HR	*p* value	HR	*p* value	HR	*p* value	HR	*p* value
Age	1.03 (1.01, 1.05)	0.013	1.02 (0.99, 1.05)	0.082	1.02 (0.99, 1.04)	0.129	1.01 (0.99, 1.04)	0.276
KPS	0.99 (0.96, 1.01)	0.300	0.99 (0.96, 1.02)	0.437	0.99 (0.97, 1.02)	0.555	0.99 (0.97, 1.02)	0.667
Extent of resection	0.51 (0.19, 1.37)	0.183	0.41 (0.15, 1.14)	0.086	0.43 (0.15, 1.18)	0.100	0.37 (0.13, 1.04)	0.058
IDH mutation					0.26 (0.07, 0.89)	0.032	0.32 (0.09, 1.13)	0.078
APT signal			2.13 (1.21, 3.75)	0.009			2.00 (1.11, 3.60)	0.022
Original iAUC	0.663 (0.568, 0.756)		0.716 (0.624, 0.810)		0.697 (0.608, 0.782)		0.736 (0.656, 0.823)	
Difference of iAUC	0.053 (0.004, 0.128)				0.039 (0.002, 0.103)			
Bootstrapped iAUC	0.681 (0.591, 0.779)		0.737 (0.641, 0.837)		0.722 (0.639, 0.820)		0.766 (0.677, 0.874)	
Difference of bootstrapped iAUC	0.055 (0.013, 0.137)				0.043 (0.007, 0.121)			

Numbers in parentheses indicate the 95% confidence interval. *HR* = hazard ratio. *KPS* = Karnofsky performance status score. *MGMT* = O^6-methylguanine-DNA methyltransferase. *IDH* = isocitrate dehydrogenase. *APT* = amide proton transfer. *iAUC* = integrated AUC

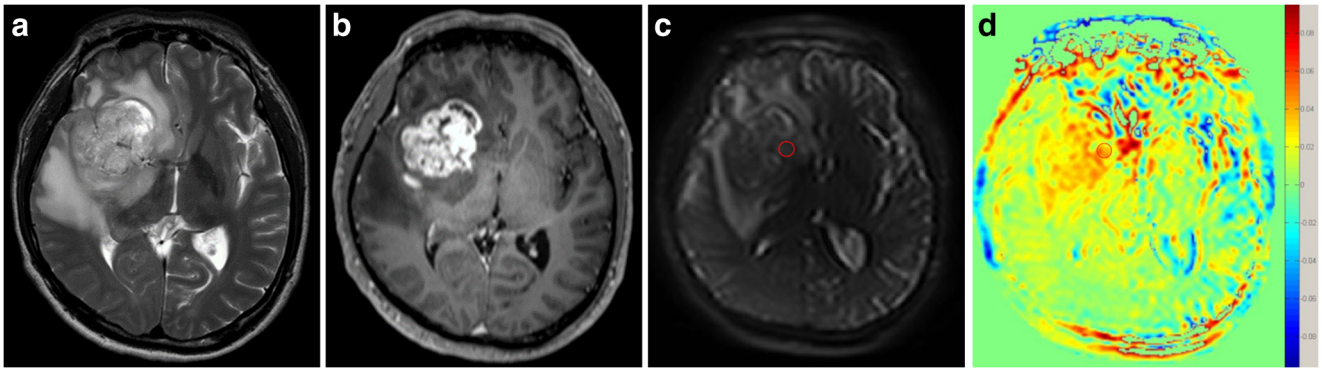

Fig. 2 A 42-year-old male patient with an IDH-wild-type glioblastoma without MGMT methylation (WHO grade IV) at the right frontal lobe showing infiltrative mass with perilesional edema on a T2-weighted image (**a**) and strong and heterogeneous enhancement on a contrast-enhanced T1-weighted image (**b**). ROI was drawn on area which showed the highest signal within the lesion on a raw APT image (**c**) and then transferred to the processed APT-weighted image (**d**). The APT signal was 3.44%, which belongs to the higher APT signal groups according to the optimized cutoff values for OS and PFS prediction. The PFS and OS of this patient were 264 and 363 days, respectively

[25, 36]. Previous studies are thought to be consistent with the assumption; higher APT signals reflect an increase in tumor cellularity and proliferation, and aggressiveness [28, 32, 37, 38]. This correlation between APT signals and tumor aggressiveness in previous studies are in line with our findings that a higher APT signal was significantly related to poor prognosis.

In our study, even after adjusting for molecular markers and clinical factors, APT signal was the only independent prognostic factor for both OS and PFS. Old age, wild-type IDH, MGMT promoter unmethylation, and high APT signals were associated with poor OS in the univariate analyses, consistent with previous reports [3, 6–9]. However, APT signal was the only significant prognostic factor for OS in the multivariate analysis. There were similar results in the PFS analysis. According to the "cutp" function of the "survMisc" R, the optimal values of APT-weighted signal for OS and PFS prediction were 2.22 and 2.30, respectively. On the other hand, the mean and median values of APT signals of our study were 2.23 and 2.30, respectively. Considering that the gap between the calculated optimal values and mean/median values is minimal, we suppose that our conclusion that high APT signals indicate poor prognosis can be generalized in other clinical settings. Interestingly, MGMT methylation status was associated with OS but not with PFS. This is in line with a previous meta-analysis, which showed that OS was prolonged, but there was no improvement in PFS, in patients with glioblastoma with the methylated MGMT promoter [39]. In contrast, IDH mutation was a significant predictor of both OS and PFS in our univariate analysis.

The incremental prognostic value of APT imaging over clinical and molecular factors was evaluated by iAUC. We found that models including APT signal as a factor showed significant incremental prognostic value over models without APT signal for both OS and PFS, which was validated by the internal validation analysis. This result implies that preoperative APT imaging is highly valuable, given that molecular marker status is available only after biopsy or tumor resection.

Regarding the molecular markers and APT signals, we found that APT signals are associated with IDH mutation status. This is consistent with recent studies that have used APT imaging to predict IDH mutation status in grade II gliomas [29, 31]. IDH gene–encoded enzymes are involved in a number of cellular functions, including amino acid metabolism, lipid metabolism,

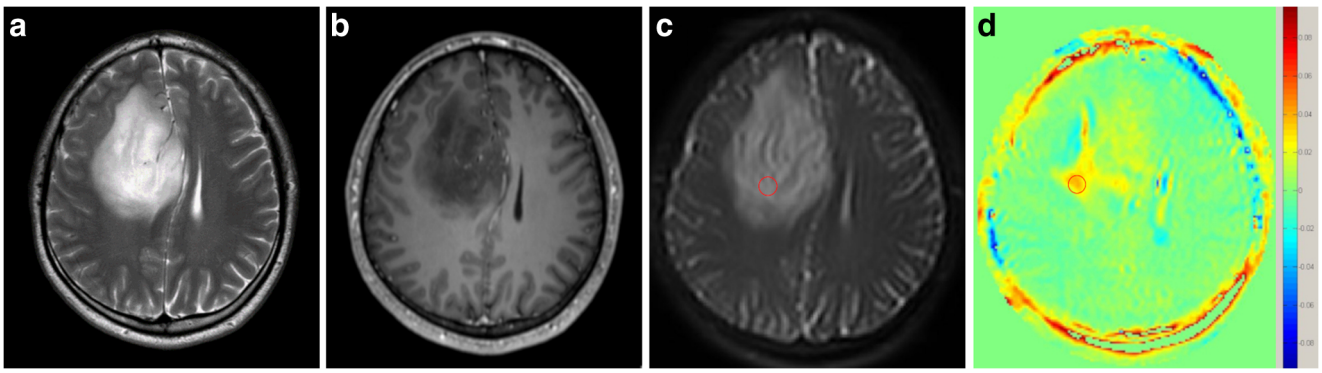

Fig. 3 A 27-year-old male patient with an IDH-mutant anaplastic astrocytoma with MGMT methylation (WHO grade III) at the right frontal lobe showing relatively homogeneous signal intensity on a T2-weighted image (**a**) and minimal enhancement on a contrast-enhanced T1-weighted image (**b**). A ROI was drawn on solid portion of the tumor on a raw APT image (**c**) and then transferred to the processed APT-weighted image (**d**). The APT signal was 2.37%, which belongs to the higher APT signal groups according to the optimized cutoff values for OS and PFS prediction. The PFS and OS of this patient were 387 and 779 days, respectively

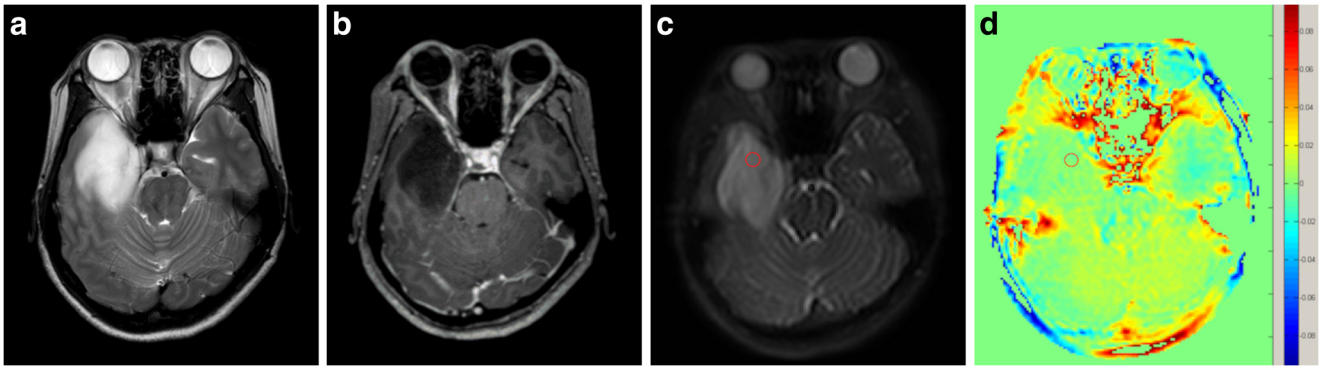

Fig. 4 A 38-year-old woman with an IDH-mutant anaplastic astrocytoma with MGMT methylation (WHO grade III) at the right temporal lobe showing homogeneous high signal intensity on a T2-weighted image (**a**) and no enhancement on a contrast-enhanced T1-weighted image (**b**). ROI was drawn on area which showed the highest signal within the lesion on a raw APT image (**c**) and then transferred to the processed APT-weighted image (**d**). The APT signal was 1.58%, which belongs to the lower APT signal groups according to the optimized cutoff values for OS and PFS prediction. The PFS of this patient was 921 days. This patient was alive at the last follow-up

regulation of cellular redox status, and cellular epigenetics and genome-wide DNA methylation [17]. Therefore, IDH mutation is thought to cause alteration of amide acid concentrations, global transcriptional repression, and overall downregulation of protein expression, which could explain our findings [40, 41]. Further studies are needed to further elucidate the biochemical origin of the changes in APT signals regarding IDH mutation in glioma.

We did not find a significant difference in APT signals associated with MGMT methylation, which is consistent with a previous study where authors found that APT imaging enabled the prediction of IDH mutation, but not MGMT methylation, status [31]. Interestingly, another study has reported that APT imaging provided valuable information for the discrimination of MGMT methylation status in glioblastomas [30]. However, these studies were performed under different settings with different patient populations, image acquisition parameters, image processing, and analyses. Therefore, further investigation is needed to confirm the utility of APT imaging in predicting molecular marker status in glioma.

In many prior studies with APT imaging in brain tumor, it has been presumed that the increased APT signal comes from an increase in the exchangeable amide proton due to a higher protein content in tumors [25–29, 38, 42, 43]. However, other effects can contribute to the amplitude of the signal, including nuclear Overhauser enhancement (NOE), conventional semisolid magnetization transfer asymmetry, intracellular pH, water longitudinal relaxation time, and water concentration. Image acquisition methods, such as duration and amplitude of saturation RF pulse, can also affect the signal [44–46]. However, a recent study which investigated the APT, NOE, and MTR_{asym} signal features and their relationships in malignant glioma in rat model validated the reliability of MTR_{asym} values at ± 3.5 as an APT imaging metric, which we used in the current study [47]. Regarding this issue, further investigation with various APT metrics needs to be explored in the future for application of APT imaging in clinical practice.

In addition to the retrospective study design, several limitations should be mentioned. First, although MTR_{asym} was reported to be a promising and reliable metric for CEST imaging [47], there could be a possibility of unanticipated effects to our results from varying image acquisition parameters. Recently, alternative metrics and image acquisition methods are under investigation and expected to be helpful for more reliable application of APT imaging in clinical practice with exact quantitative explanation [31, 32, 46–48]. Second, precise locus-specific pathologic-radiologic correlations were not made. However, most patients underwent total tumor resection (62 out of 71 patients); therefore, the possibility of under-sampling was low in this study. Third, ROIs were placed manually in the solid portions of tumors, which we considered representative of tumor characteristics. We chose to use the hot spot method, due to the limited spatial resolution of APT imaging, for co-registration. Additionally, a previous study showed comparable results of hot spot method to whole tumor analysis for glioma

Table 5 Differences in APT signal according to IDH mutation and MGMT methylation status

	IDH mutation status		MGMT methylation status	
	IDH-wild type	IDH-mutant	Unmethylated	Methylated
APT signal (%)	2.42 (2.21–2.64)	1.60 (0.97–2.23)	2.41 (2.16–2.66)	2.17 (1.74–2.49)
p value	0.001		0.208	

APT signal data are presented as the median (interquartile range). *MGMT* = O^6-methylguanine-DNA methyltransferase. *IDH* = isocitrate dehydrogenase. *APT* = amide proton transfer

grading [49]. Fourth, our sample size was relatively small ($N = 71$); therefore, we used internal validation with the bootstrap procedure to overcome this limitation. Further studies with a larger population may be necessary to validate our results. Fifth, two different MRI scanners were used for this study as one of the scanners was replaced with the other in the middle of the study. The parameters used in this study were exactly the same for the two scanners. However, our results might have been affected by the difference in scanner performance. Further studies regarding the performance differences of CEST imaging according to different scanners would be required, especially for the standardization of CEST imaging. Finally, among the patients with WHO grade IV glioma, only one patient had IDH mutation. However, considering that IDH mutations are present in approximately 5% of glioblastomas [15], this result was inevitable. Furthermore, because the number of IDH-mutant WHO IV case was only one, we thought adjusting for both tumor grade and IDH mutation in Cox analysis would be unreliable. Therefore, between the two factors, we decided to choose only IDH mutation as a covariate, based on a study reporting that the IDH mutation status is more prognostic for overall survival than standard histological criteria in high-grade astrocytomas [50]. Nonetheless, this might have affected our analysis as a confounding factor. Further investigations with more IDH-mutant glioblastoma cases would be required to obtain more conclusive results.

In conclusion, we investigated the usefulness of APT imaging as a prognostic biomarker of HGG. We found that high APT signals were a significant predictor of poor prognosis. APT imaging data showed significant incremental prognostic value over standard clinical prognostic and molecular markers. Further, APT signals may predict IDH mutation status in HGG. Hence, preoperative APT imaging is a valuable imaging biomarker for predicting the prognosis and IDH mutation status of patients with HGG.

Acknowledgements The authors thank Ha-Kyu Jeong (Korea Basic Science Institute, Chungcheongbuk-do, Korea) for his help with protocol optimization and for the valuable suggestions.

Funding This research received funding from the Basic Science Research Program through the National Research Foundation of Korea (NRF) funded by the Ministry of Science, ICT and Future Planning (2014R1A1A1002716, 2017R1D1A1B03030440) and National Institutes of Health (P41 EB015909, R01 CA166171, R01 EB009731).

Compliance with ethical standards

Guarantor The scientific guarantor of this publication is Professor Seung-Koo Lee, MD, PhD, from Yonsei University College of Medicine.

Conflict of interest The authors of this manuscript declare no relationships with any companies, whose products or services may be related to the subject matter of the article.

Statistics and biometry One of the authors has significant statistical expertise.

Kyunghwa Han, PhD

Department of Radiology and Research Institute of Radiological Science, College of Medicine, Yonsei University College of Medicine, Seoul, Korea.

Informed consent The institutional review board waived the requirement to obtain informed patient consent for this retrospective study.

Ethical approval Institutional Review Board approval was obtained.

Methodology
- retrospective
- diagnostic or prognostic study
- performed at one institution

References

1. Ricard D, Idbaih A, Ducray F, Lahutte M, Hoang-Xuan K, Delattre JY (2012) Primary brain tumours in adults. Lancet 379:1984–1996
2. Stupp R, Brada M, van den Bent MJ, Tonn JC, Pentheroudakis G (2014) High-grade glioma: ESMO clinical practice guidelines for diagnosis, treatment and follow-up. Ann Oncol 25:iii93–iii101
3. Lamborn KR, Chang SM, Prados MD (2004) Prognostic factors for survival of patients with glioblastoma: recursive partitioning analysis. Neuro Oncol 6:227–235
4. Mirimanoff RO, Gorlia T, Mason W et al (2006) Radiotherapy and temozolomide for newly diagnosed glioblastoma: recursive partitioning analysis of the EORTC 26981/22981-NCIC CE3 phase III randomized trial. J Clin Oncol 24:2563–2569
5. Brown TJ, Brennan MC, Li M et al (2016) Association of the extent of resection with survival in glioblastoma: a systematic review and meta-analysis. JAMA Oncol 2:1460–1469
6. Zou P, Xu H, Chen P et al (2013) IDH1/IDH2 mutations define the prognosis and molecular profiles of patients with gliomas: a meta-analysis. PLoS One 8:e68782
7. Weller M, Tabatabai G, Kästner B et al (2015) MGMT promoter methylation is a strong prognostic biomarker for benefit from dose-intensified temozolomide rechallenge in progressive glioblastoma: the DIRECTOR trial. Clin Cancer Res 21:2057–2064
8. Leu S, von Felten S, Frank S et al (2013) IDH/MGMT-driven molecular classification of low-grade glioma is a strong predictor for long-term survival. Neuro Oncol 15:469–479
9. Yang F, Yang P, Zhang C et al (2017) Stratification according to recursive partitioning analysis predicts outcome in newly diagnosed glioblastomas. Oncotarget 8:42974–42982
10. Brat DJ, Verhaak RG, Aldape KD et al (2015) Comprehensive, integrative genomic analysis of diffuse lower-grade gliomas. N Engl J Med 372:2481–2498
11. Ludwig K, Kornblum HI (2017) Molecular markers in glioma. J Neurooncol 134:505–512
12. Tateishi K, Wakimoto H, Cahill DP (2017) IDH1 mutation and World Health Organization 2016 diagnostic criteria for adult diffuse gliomas: advances in surgical strategy. Neurosurgery 64:134–138
13. Siegal T (2016) Clinical relevance of prognostic and predictive molecular markers in gliomas. Adv Tech Stand Neurosurg. https://doi.org/10.1007/978-3-319-21359-0_4:91-108
14. Yan H, Parsons DW, Jin G et al (2009) IDH1 and IDH2 mutations in gliomas. N Engl J Med 360:765–773
15. Miller JJ, Shih HA, Andronesi OC, Cahill DP (2017) Isocitrate dehydrogenase-mutant glioma: evolving clinical and therapeutic implications. Cancer 123:4535–4546
16. Louis DN, Perry A, Reifenberger G et al (2016) The 2016 World Health Organization classification of tumors of the central nervous system: a summary. Acta Neuropathol 131:803–820

17. Waitkus MS, Diplas BH, Yan H (2016) Isocitrate dehydrogenase mutations in gliomas. Neuro Oncol 18:16–26
18. Baldewpersad Tewarie NM, Burgers IA, Dawood Y et al (2013) NADP+ -dependent IDH1 R132 mutation and its relevance for glioma patient survival. Med Hypotheses 80:728–731
19. Hegi ME, Diserens A-C, Gorlia T et al (2005) MGMT gene silencing and benefit from temozolomide in glioblastoma. N Engl J Med 352:997–1003
20. Pope WB, Sayre J, Perlina A, Villablanca JP, Mischel PS, Cloughesy TF (2005) MR imaging correlates of survival in patients with high-grade gliomas. AJNR Am J Neuroradiol 26:2466–2474
21. Hirai T, Murakami R, Nakamura H et al (2008) Prognostic value of perfusion MR imaging of high-grade astrocytomas: long-term follow-up study. AJNR Am J Neuroradiol 29:1505–1510
22. Choi YS, Ahn SS, Kim DW et al (2016) Incremental prognostic value of ADC histogram analysis over MGMT promoter methylation status in patients with glioblastoma. Radiology 281:175–184
23. Ulyte A, Katsaros VK, Liouta E et al (2016) Prognostic value of preoperative dynamic contrast-enhanced MRI perfusion parameters for high-grade glioma patients. Neuroradiology 58:1197–1208
24. Ward KM, Aletras AH, Balaban RS (2000) A new class of contrast agents for MRI based on proton chemical exchange dependent saturation transfer (CEST). J Magn Reson 143:79–87
25. Zhou J, Lal B, Wilson DA, Laterra J, van Zijl PC (2003) Amide proton transfer (APT) contrast for imaging of brain tumors. Magn Reson Med 50:1120–1126
26. Jones CK, Schlosser MJ, van Zijl PC, Pomper MG, Golay X, Zhou J (2006) Amide proton transfer imaging of human brain tumors at 3T. Magn Reson Med 56:585–592
27. Choi YS, Ahn SS, Lee SK et al (2017) Amide proton transfer imaging to discriminate between low- and high-grade gliomas: added value to apparent diffusion coefficient and relative cerebral blood volume. Eur Radiol 27:3181–3189
28. Togao O, Yoshiura T, Keupp J et al (2014) Amide proton transfer imaging of adult diffuse gliomas: correlation with histopathological grades. Neuro Oncol 16:441–448
29. Jiang S, Zou T, Eberhart CG et al (2017) Predicting IDH mutation status in grade II gliomas using amide proton transfer-weighted (APTw) MRI. Magn Reson Med 78:1100–1109
30. Jiang S, Rui Q, Wang Y et al (2018) Discriminating MGMT promoter methylation status in patients with glioblastoma employing amide proton transfer-weighted MRI metrics. Eur Radiol 28:2115–2123
31. Paech D, Windschuh J, Oberhollenzer J et al (2018) Assessing the predictability of IDH mutation and MGMT methylation status in glioma patients using relaxation-compensated multi-pool CEST MRI at 7.0 Tesla. Neuro Oncol. https://doi.org/10.1093/neuonc/noy073
32. Regnery S, Adeberg S, Dreher C et al (2018) Chemical exchange saturation transfer MRI serves as predictor of early progression in glioblastoma patients. Oncotarget 9:28772
33. Kim M, Gillen J, Landman BA, Zhou J, van Zijl PC (2009) Water saturation shift referencing (WASSR) for chemical exchange saturation transfer (CEST) experiments. Magn Reson Med 61:1441–1450
34. Choi J, Lee EY, Shin KJ, Minn YK, Kim J, Kim SH (2013) IDH1 mutation analysis in low cellularity specimen: a limitation of diagnostic accuracy and a proposal for the diagnostic procedure. Pathol Res Pract 209:284–290
35. Heagerty PJ, Zheng Y (2005) Survival model predictive accuracy and ROC curves. Biometrics 61:92–105
36. Yan K, Fu Z, Yang C et al (2015) Assessing amide proton transfer (APT) MRI contrast origins in 9 L gliosarcoma in the rat brain using proteomic analysis. Mol Imaging Biol 17:479–487
37. Su C, Liu C, Zhao L et al (2017) Amide proton transfer imaging allows detection of glioma grades and tumor proliferation: comparison with Ki-67 expression and proton MR spectroscopy imaging. AJNR Am J Neuroradiol 38:1702–1709
38. Park JE, Kim HS, Park KJ, Kim SJ, Kim JH, Smith SA (2016) Pre- and posttreatment glioma: comparison of amide proton transfer imaging with MR spectroscopy for biomarkers of tumor proliferation. Radiology 278:514–523
39. Binabaj MM, Bahrami A, ShahidSales S et al (2018) The prognostic value of MGMT promoter methylation in glioblastoma: a meta-analysis of clinical trials. J Cell Physiol 233:378–386
40. Doll S, Urisman A, Oses-Prieto JA, Arnott D, Burlingame AL (2017) Quantitative proteomics reveals fundamental regulatory differences in oncogenic HRAS and Isocitrate dehydrogenase (IDH1) driven astrocytoma. Mol Cell Proteomics 16:39–56
41. Reitman ZJ, Jin G, Karoly ED et al (2011) Profiling the effects of isocitrate dehydrogenase 1 and 2 mutations on the cellular metabolome. Proc Natl Acad Sci U S A 108:3270–3275
42. Zhou J, Tryggestad E, Wen Z et al (2010) Differentiation between glioma and radiation necrosis using molecular magnetic resonance imaging of endogenous proteins and peptides. Nat Med 17:130
43. Park JE, Kim HS, Park KJ, Choi CG, Kim SJ (2015) Histogram analysis of amide proton transfer imaging to identify contrast-enhancing low-grade brain tumor that mimics high-grade tumor: increased accuracy of MR perfusion. Radiology 277:151–161
44. Jones CK, Huang A, Xu J et al (2013) Nuclear Overhauser enhancement (NOE) imaging in the human brain at 7T. Neuroimage 77:114–124
45. van Zijl PC, Yadav NN (2011) Chemical exchange saturation transfer (CEST): what is in a name and what isn't? Magn Reson Med 65:927–948
46. Zaiss M, Windschuh J, Paech D et al (2015) Relaxation-compensated CEST-MRI of the human brain at 7T: unbiased insight into NOE and amide signal changes in human glioblastoma. Neuroimage 112:180–188
47. Lee DH, Heo HY, Zhang K et al (2017) Quantitative assessment of the effects of water proton concentration and water T1 changes on amide proton transfer (APT) and nuclear overhauser enhancement (NOE) MRI: the origin of the APT imaging signal in brain tumor. Magn Reson Med 77:855–863
48. Heo HY, Zhang Y, Lee DH, Hong X, Zhou J (2016) Quantitative assessment of amide proton transfer (APT) and nuclear overhauser enhancement (NOE) imaging with extrapolated semi-solid magnetization transfer reference (EMR) signals: application to a rat glioma model at 4.7 tesla. Magn Reson Med 75:137–149
49. Sakata A, Okada T, Yamamoto A et al (2015) Grading glial tumors with amide proton transfer MR imaging: different analytical approaches. J Neurooncol 122:339–348
50. Hartmann C, Hentschel B, Wick W et al (2010) Patients with IDH1 wild type anaplastic astrocytomas exhibit worse prognosis than IDH1-mutated glioblastomas, and IDH1 mutation status accounts for the unfavorable prognostic effect of higher age: implications for classification of gliomas. Acta Neuropathol 120:707–718